

Lymph node targeted immune-activation by engineered block copolymer amphiphiles - TLR7/8 agonist conjugates

Simon Van Herck, Kim Deswarte, Lutz Nuhn, zifu zhong, joao paulo portela catani, Yupeng Li, Niek N. Sanders, Stefan Lienenklaus, stefaan de koker, Bart N. Lambrecht, Sunil A. David, and Bruno G. De Geest

J. Am. Chem. Soc., **Just Accepted Manuscript** • DOI: 10.1021/jacs.8b08595 • Publication Date (Web): 02 Oct 2018

Downloaded from <http://pubs.acs.org> on October 2, 2018

Just Accepted

“Just Accepted” manuscripts have been peer-reviewed and accepted for publication. They are posted online prior to technical editing, formatting for publication and author proofing. The American Chemical Society provides “Just Accepted” as a service to the research community to expedite the dissemination of scientific material as soon as possible after acceptance. “Just Accepted” manuscripts appear in full in PDF format accompanied by an HTML abstract. “Just Accepted” manuscripts have been fully peer reviewed, but should not be considered the official version of record. They are citable by the Digital Object Identifier (DOI®). “Just Accepted” is an optional service offered to authors. Therefore, the “Just Accepted” Web site may not include all articles that will be published in the journal. After a manuscript is technically edited and formatted, it will be removed from the “Just Accepted” Web site and published as an ASAP article. Note that technical editing may introduce minor changes to the manuscript text and/or graphics which could affect content, and all legal disclaimers and ethical guidelines that apply to the journal pertain. ACS cannot be held responsible for errors or consequences arising from the use of information contained in these “Just Accepted” manuscripts.



Lymph node targeted immune-activation by engineered block copolymer amphiphiles - TLR7/8 agonist conjugates

Simon Van Herck,¹ Kim Deswarte,^{2,3} Lutz Nuhn,^{1†} Zifu Zhong,⁴ Joao Paulo Portela Catani,⁴ Yupeng Li,⁵ Niek N Sanders,⁴ Stefan Lienenklaus,⁶ Stefaan De Koker,¹ Bart N Lambrecht,^{2,3} Sunil A David,⁵ Bruno G. De Geest^{1*}

¹ Department of Pharmaceutics, Ghent University, Belgium.

² IRC-VIB, Zwijnaarde, Belgium.

³ Department of Respiratory Medicine, Ghent University, Belgium

⁴ Laboratory of Gene Therapy, Department of Nutrition, Genetics and Ethology, Faculty of Veterinary Medicine, Ghent University, Belgium

⁵ Department of Medicinal Chemistry, University of Minnesota, Minneapolis, Minnesota, United States.

⁶ Institute for Laboratory Animal Science, Hannover Medical School, Hannover, Germany.

ABSTRACT: Small molecule immuno-modulators such as agonists of Toll like receptors are attractive compounds to stimulate innate immune cells towards potent anti-viral and anti-tumor responses. However, small molecules rapidly enter systemic circulation and cause 'wasted inflammation'. Hence, synthetic strategies to confine their radius of action to lymphoid tissue are of great relevance, to both enhance their efficacy and concomitantly limit toxicity. Here we demonstrate that covalent conjugation of a small molecule TLR7/8 agonist immunomodulatory to a micelle-forming amphiphilic block copolymer greatly alters the pharmacokinetic profile, resulting in highly efficient lymphatic delivery. Moreover, we designed amphiphilic block copolymers in such way to form thermodynamically stable micelles through pi-pi stacking between aromatic moieties, and engineer the block copolymers to undergo an irreversible amphiphilic to hydrophilic transition in response to the acidic endosomal pH.

INTRODUCTION

Potent activation of dendritic cells is crucial in the context of vaccination and anti-cancer immunotherapy.^{1,2} Hereto, small molecule immuno-modulators such as agonists of Toll like receptors 7 and 8 (TLR 7/8) are an attractive class of molecules as they can trigger broad activation of innate immune cells. Thereby inducing potent cytokine responses that skew Th1 and cytotoxic T cells activation that are key effector cells in combating intracellular infections and cancer.^{3,4} However, small molecule immune modulators typically suffer from an unfavorable pharmacokinetic profile and are prone to rapid systemic dissemination and hence lead to 'wasted inflammation' and systemic toxicity. It is known that conjugation of small molecule TLR7/8 agonists to polymer nanoparticles alters the pharmacokinetic profile, and thus, enhancing safety by restricting immune-activation to secondary lymphoid tissue.⁵⁻¹⁰ Whereas this has been demonstrated for stable colloids, obtained either by chemical crosslinking or through coil-to globule formation by heating a thermoresponsive polymer above its phase transition temperature, the use of block copolymer amphiphiles to target lymphoid tissue, despite their appealing inherent simplicity. Indeed, block copolymers have the advantage over the aforementioned systems as

they are easy to manufacture, allow for controlled assembly into micellar nanoparticles and can be engineered to be responsive to environmental triggers. In particular, compared to core-crosslinked nanogel structures earlier reported by us,⁵ amphiphilic block copolymer micelles excel in simplicity as the crosslinking step itself, with its inherent variability and residual non-crosslinked repeating moieties, is omitted and compatibility issues between crosslinking chemistry and the biologically active molecule of interest are avoided. An often employed trigger is the endosomal pH, by introduction of acid-degradable bonds polymer solubilization can be achieved leading to hydrophilic polymer degradation products that can be secreted through the body.¹¹⁻¹⁵

As soluble polymers exhibit poor lymphatic drainage,^{16,17} we envisioned that block copolymer amphiphiles with high thermodynamic and kinetic stability would favor lymphatic transportation. In this regard, benzyl groups as repeating units along the hydrophobic polymer block are attractive as they are able to tightly associate through pi-pi stacking.¹⁸ Here we report on novel highly stable, but acid-degradable block copolymer amphiphiles that can modulate the pharmacokinetic profile of a small molecule immunomodulator.

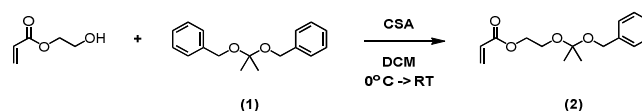
RESULTS AND DISCUSSION

Benzyl alcohol is a non-toxic aromate that is commonly used in commodity products, hence we opted for this compound as building block for a novel monomer 2-((2-(benzyloxy)propan-2-yl)oxy)ethyl acrylate (BzKEA, **2**) that combines a polymerizable acrylate moiety with a benzyl moiety through an acid-degradable ketal linker. As depicted in **Scheme 1** and **Scheme S1**, in a first step, the symmetrical benzylalcohol based ketal, 2,2-dibenzoyloxypropane (**1**) is obtained by transacetalization of benzylalcohol and 2,2-dimethoxypropane catalyzed by camphorsulfonic acid (CSA). In a second transacetalization step, replacement of one benzyloxy with 2-hydroxyethyl acrylate (HEA) yielded the monomer (**2**, further denoted as BzKEA) as confirmed by NMR and MS (**Figure S1**).

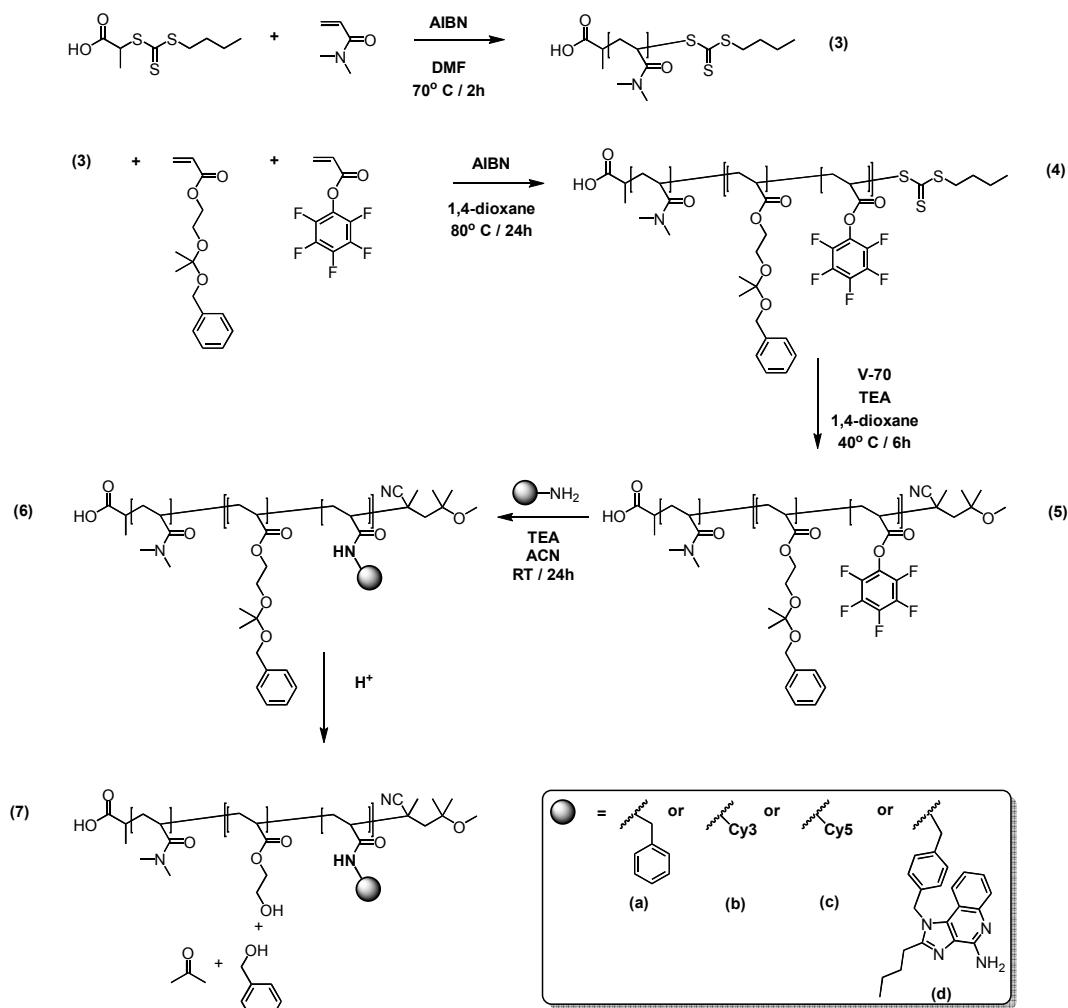
Reversible addition-fragmentation chain transfer (RAFT) polymerization (**Scheme 2**) was used to synthesize well-defined block copolymer amphiphiles using poly(*N,N*-dimethylacrylamide) (pDMA) as macro chain transfer agent (macroCTA, **3**). Note that pDMA was chosen for its hydrophilic and biocompatible properties.¹⁹ To allow for further conjugation of a fluorescent tracer

and/or TLR7/8 agonist immunomodulator, chain extension of the macroCTA was achieved by copolymerizing 15 mol% of pentafluorophenylacrylate (PFPA) with BzKEA, targeting an overall DP of 40. An overview of polymerization conditions as well as NMR and SEC analysis is provided in **Table S1** and **Figure S2-4**, respectively. No detailed investigation was done on the copolymerization kinetics. However, the similar monomer conversion obtained in reactions stopped at different time points prove strong evidence for random copolymer formation (*cf.* **Table S2**). After polymerization the trithiocarbonate RAFT end-group was removed by reacting the polymer with an excess of the low-temperature azo-initiator V-70, to avoid later on uncontrolled side reaction by polymer end-group thiol/disulfide formation.

Scheme 1. Synthesis scheme of benzyl modified 2-hydroxyethylacrylate (BzKEA).



Scheme 2. Synthesis of pDMA-*block*-(BzKEA-PFPA) by RAFT polymerization, trithiocarbonate end-group removal and substitution of activated PFP-esters with functional amines. Acid triggered hydrolysis of the ketal bond affords the hydrophilic block copolymer.



The obtained block polymer amphiphile scaffold **5** was used for conjugation by amide bond formation with the imidazoquinoline TLR7/8 agonist IMDQ and/or the fluorophores Cy3 and Cy5 (**Scheme 1**). A control polymer was synthesized by converting the PFP-ester moieties with benzylamine. To obtain hydrophilic block polymers without amphiphilic properties, the benzyl side chains were removed by acidic hydrolysis of the ketal bonds that connect the benzyl groups to the polymer backbone. ¹H-NMR spectroscopy confirms the disappearance of the benzylic and ketal group (**Figure S3**) upon exposure to acidic conditions. Dynamic light scattering (DLS, **Figure 1 and Figure S5**) in aqueous medium of the block copolymer amphiphiles indicated the formation of 50 nm sized micellar nanoparticles. When dispersed in buffer at pH 5 unimers with sizes below 10 nm were found over time (**Figure 1**) due to ketal hydrolysis and formation of hydrophilic block copolymers. **Table 1** lists all obtained polymers with their molecular and physicochemical properties. For the sake of simplicity, we will use **amph** as abbreviation to refer to amphiphilic block copolymers and **hydro** to refer to their hydrolyzed hydrophilic counterpart.

Amph labeled with either Cy3 or Cy5 were used to prepare micelles that exhibit Förster Resonance Energy

Transfer (FRET) (**Figure 2A**).²⁰ In aqueous solution, fluorescence

spectroscopy (**Figure 2B and Figure S6**) showed strong FRET coupling between Cy3 and Cy5 (emission at 675 nm (λ_{max} of Cy5), excitation at 550 nm (λ_{max} of Cy3)) in case of amphiphilic block copolymer micelles (**amph^{Cy3/Cy5}**). The complete absence of FRET coupling upon ketal hydrolysis (i.e. **hydro^{Cy3/Cy5}**) provides proof that the FRET signal is due to micellar self-assembly and not merely due to presence of both dyes. FRET and DLS analysis were used to investigate pH dependent micelle dissociation at pH values of 7.4 (i.e. physiological pH) and 5 (endosomal pH). DLS (**Figure 1**) indicated rapid disassembly at pH 5, characterized by a decrease in scattering intensity and a decrease in size over time, whereas at the neutral pH of 7.4, much slower kinetics were observed. A similar trend was observed when monitoring the FRET ratio (calculated as the ratio between emission of the acceptor Cy5 dye (i.e. 675 nm) and the emission of the donor Cy3 dye (i.e. 580 nm) (upon excitation of Cy3 (i.e. 550 nm)) over time (**Figure 2B**). Micelle disassembly at pH 5 is witnessed by an increase in Cy3 emission intensity resulting in a decrease in FRET coupling. Again, this behavior was strongly pH dependent with much faster kinetics at lower pH.

Table 1. Characterization of block copolymer amphiphiles (*amph*) and hydrophilic (*hydro*) block copolymers.

block copolymer	Modification	M_n^{sec} (kDa)	M_n^{theor} (kDa)	\bar{D}	Hydrodynamic average (nm)	Z-	Volume mean (nm)	PdI
pDMA ₄₆ (BenKEA ₃₂ PFPA ₅)	/	8.7	14.4	1.26				
amph ^{Bz}	benzylamine	9.0	14.0	1.26	53 ± 0.3		44 ± 0.5	0.11 ± 0.01
hydro ^{Bz}	benzylamine + HCl	8.4	9.3	1.33	82 ± 18		4.5 ± 0.2	0.94 ± 0.11
amph ^{Cy3}	Cy3-amine	9.6	14.5	1.25	34 ± 0.6		35 ± 3	0.37 ± 0.01
hydro ^{Cy3}	Cy3-amine + HCl				130 ± 53		4.9 ± 1	0.75 ± 0.29
amph ^{Cy5}	Cy5-amine				*		*	*
hydro ^{Cy5}	Cy5-amine + HCl				*		*	*
amph ^{IMDQ}	IMDQ				69 ± 0.9		53 ± 1.7	0.16 ± 0.02
hydro ^{IMDQ}	IMDQ + HCl				52 ± 32		4.3 ± 0.4	0.81 ± 0.39

*: Due to experimental set up with a wavelength operating at 633 nm, Cy5 labeled polymers/ micelles could not be characterized by DLS.

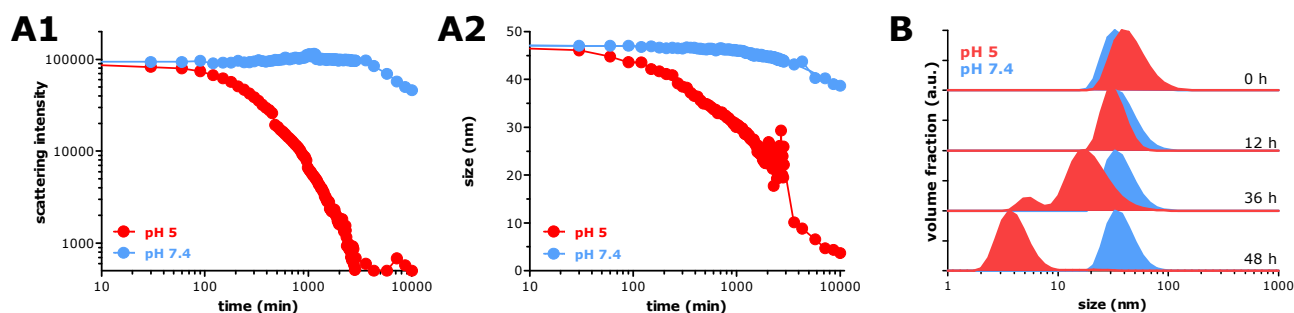


Figure 1. DLS analysis of the evolution over time for *amph*^{Bz} in buffers at pH 5 and pH 7.4. Light scattering intensity (A1) and size (A2) in response to neutral and acidic pH. (B) Corresponding size distribution at selected time points.

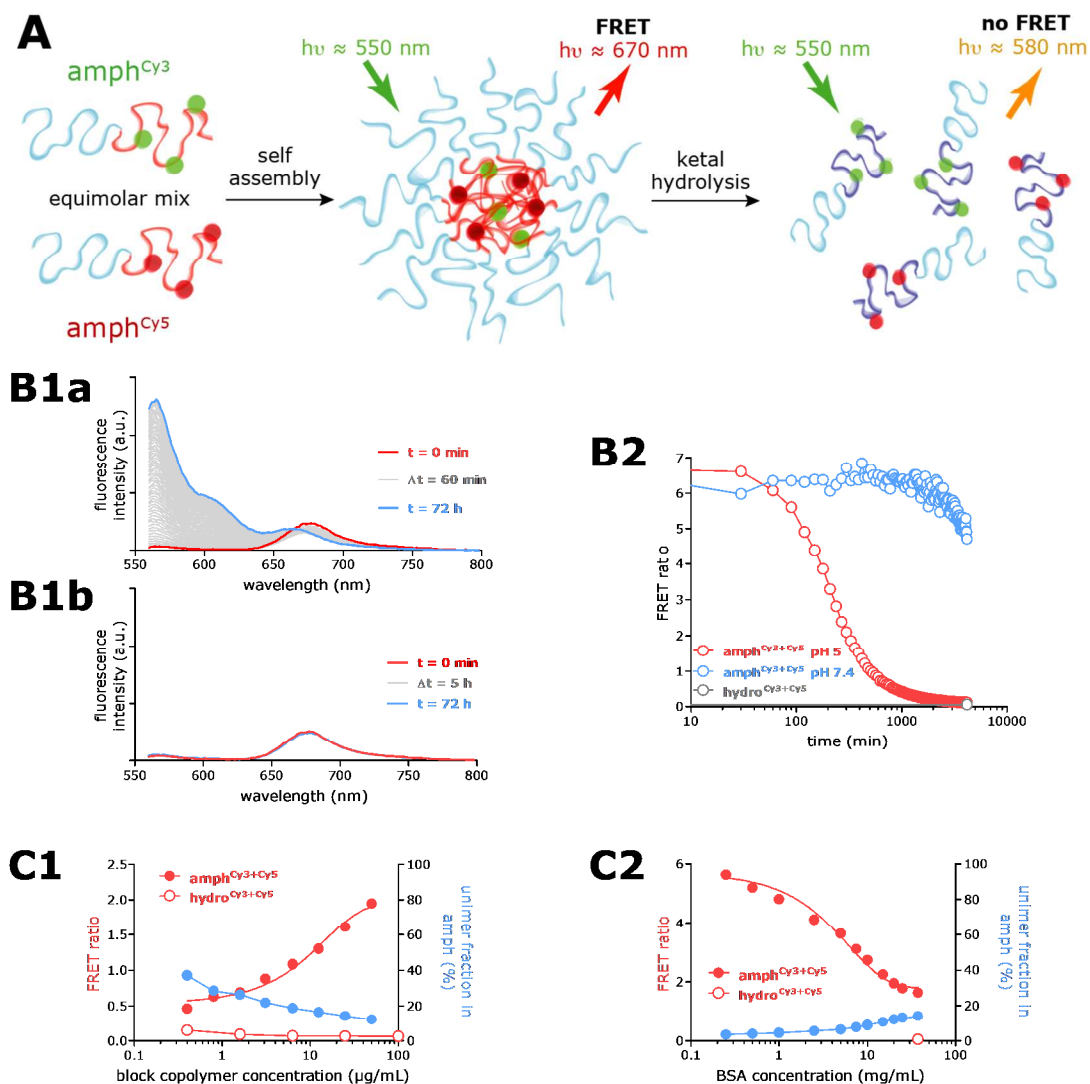


Figure 2. (A) Principle of FRET illustrated for assembly of *amph* into micelles that promote FRET coupling, and hydrolysis-induced disassembly of micelles into *hydro* with concomitant loss of FRET. (B) Evolution over time of the emission spectrum upon excitation at 550 nm at pH 5 (B1a) and pH 7.4 (B1b) and corresponding evolution of the FRET ratio. (C) FRET ratio and unimer fraction (only for *amph*) at increasing (C1) polymer and (C2) BSA concentration.

Subsequently, we used the FRET mechanism to study the behavior of the micellar nanoparticles in complex physiological media.^{21,22} The emission spectrum upon excitation at 550 nm of $amph^{Cys3/Cys5}$ was analyzed in presence of bovine serum albumin (BSA) and fetal bovine serum (FBS). The FRET ratio was then used to calculate the extent of micelle assembly. The emission spectra of $amph^{Cys3/Cys5}$, both in phosphate buffered saline (PBS) supplemented with 10 mg/mL BSA or with 10 % (v/v) FBS, show a small increase in Cy3 emission intensity (Figure S7). This resulted in a sharp decrease in FRET coupling as shown in Figure 2C. However, translated to the amount of polymer in solution, calculated with the method described in supplementary information (Figure S10). Only a very limited fraction (< 10 wt %) of $amph^{Cys3+Cys5}$ was found to be in unimer state, indicating high stability of the micellar assembly. An explanation for this trend in the FRET value could be linked to fluorescence quenching

in the micelle core (Figure S6-8). Indeed, block copolymers in unimer state exhibit much higher fluorescence emission intensity compared to equal amount of block copolymer in micelle state. Micelle-to-unimer disassembly alleviates this quenching, hence resulting in higher emission intensity and in a quick decrease in FRET coupling. Notably, the presence of serum proteins did not alter the pH dependent degradation of the polymers (Figure S8), as micelles remained stable at physiological pH for multiple days in presence of serum, whereas they rapidly disassemble in response to a pH value of 5. Further evidence of the high stability in presence of serum proteins was obtained by analyzing the FRET ratio at decreasing block copolymer concentration (Figure 2C1) or at increasing concentration of BSA (Figure 2C2). Down to block copolymer concentration as low as 0.4 $\mu\text{g/mL}$, still 60 % of the block copolymer is in micelle-assembled state, hinting at a very low CMC of the block copolymer

in serum. When measuring the FRET ratio in presence of increasing BSA concentration up to 40 mg/mL (approximate albumin concentration in serum), the FRET ratio decreased from 6 to 1.6. However, the corresponding fraction of block copolymer unimers remained below 20 %. These findings provide strong evidence for the inability of albumin or other serum proteins to promote micelle disassembly, a feature which has widely been reported for block copolymer micelles based on aliphatic hydrophobic repeating units.²³

In a next step, we investigated the behavior of *amph* in an *in vitro* cell culture setting, focusing on micelle stability, intracellular disassembly and immune-activation by the conjugated TRL7/8 agonist. Cellular uptake of *amph*^{Cy5} by dendritic cells (DCs) was visualized by confocal

microscopy. As shown in **Figure 3A**, counter-staining of endosomes with LysoTracker revealed strong colocalization with the Cy5 signal of the micelles, indicating uptake by endocytosis and accumulation in acidic intracellular vesicles.²⁴ This finding is advantageous due to the endosomal localization of TLR7/8.⁴ Flow cytometry indicated a slightly higher degree of cellular uptake of *amph*^{Cy5} compare to *hydro*^{Cy5} (**Figure 3B**). The decrease in mean fluorescence value over time is due to cell proliferation and division of the fluorescence over the daughter cells. Also note that owing to fluorescence quenching of the dye in the micelle core the extent of cellular uptake of *amph*^{Cy5} might be underestimated.

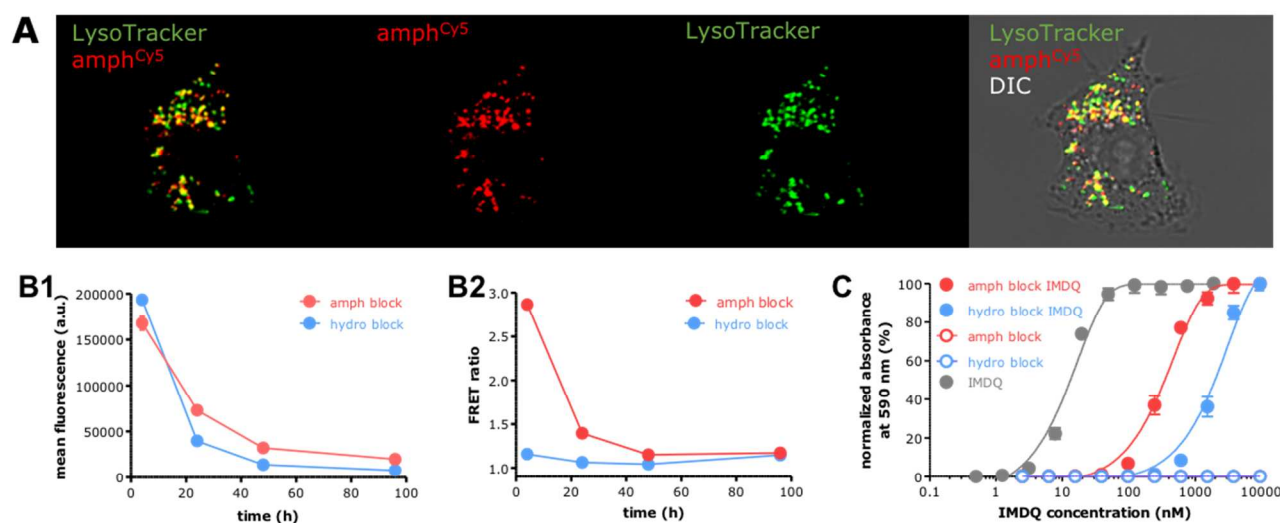


Figure 3. (A) Confocal microscopy image of dendritic cells (DC2.4) pulsed with *amph*^{Cy5} (red color). Counterstaining was done with LysoTracker (green color). (B) Intracellular (B1) Cy5 fluorescence and (B2) FRET ratio measured by FACS at multiple time points of dendritic cells (DC2.4) pulsed with *amph*^{Cy3+Cy5} (red) or *hydro*^{Cy3+Cy5} (blue). (C) TLR agonistic activity measured as NF- κ B activation in RAW-Blue cells and analyzed by Quanti-Blue reporter assay. (n = 6, mean + SD).

To investigate whether the micelles remain intact or disassemble over time inside cells, we performed flow cytometry (FACS) experiments by pulsing DCs with *amph*^{Cy3+Cy5} for 4h to allow for endocytosis to occur, followed by washing to remove non-cell associated micelles. Subsequently, cells were analyzed by FACS at different time points post-incubation and the FRET coupling inside cells was calculated. As a control, acid-hydrolyzed *hydro*^{Cy3+Cy5} unimers were used. As depicted in **Figure 3B2**, at 4 h post-incubation, a strong FRET coupling could be observed for *amph*^{Cy3+Cy5}, whereas barely a signal could be observed for *hydro*^{Cy3+Cy5}. These findings gave a first indication that the block copolymer amphiphiles were mainly taken up in intact micellar state, while only a slight difference in uptake between amphiphilic and hydrophilic block copolymers was observed (**Figure 3B1**). Monitoring

the FRET ratio as function of time, showed a rapid decrease towards values equal to those of the soluble unimers (**Figure 3B2**). This further supports the hypothesis that the block copolymer amphiphiles are endocytosed in micellar state and subsequently disassemble, mediated by ketal-hydrolysis due to the acidic endosomal pH. Endosomal hydrolysis of a similar acetone derived ketal was recently shown by us.¹⁵

Being confirmed that the micelles efficiently reach the endosomal compartment of DCs, we were interested if the TLR7/8 agonist IMDQ that is covalently linked to the hydrophobic polymer block is able to trigger TLR signaling. Hereto, we used a RAW-Blue macrophage reporter cell line, engineered to produce secreted embryonic alkaline phosphatase (SEAP) in response to TLR triggering and downstream signalling via the NF- κ B pathway. Interestingly, *amph*^{IMDQ} was one log more potent than *hydro*^{IMDQ} (**Figure 3C**), which could be attributed to the higher cellular uptake of the micelles, relative to unimers (*cf.* 48h

time point in **Figure 3B1**). In line with previous reports by us and others, a decrease in potency upon conjugation to a carrier, was observed compared to soluble IMDQ.^{5,16} Note that control *amph^{Bz}* and *hydro^{Bz}*, which did not

contain IMDQ, were totally quiescent. In parallel, the cytotoxicity of the samples was evaluated and none of them was found toxic within the tested experimental window (**Figure S16**).

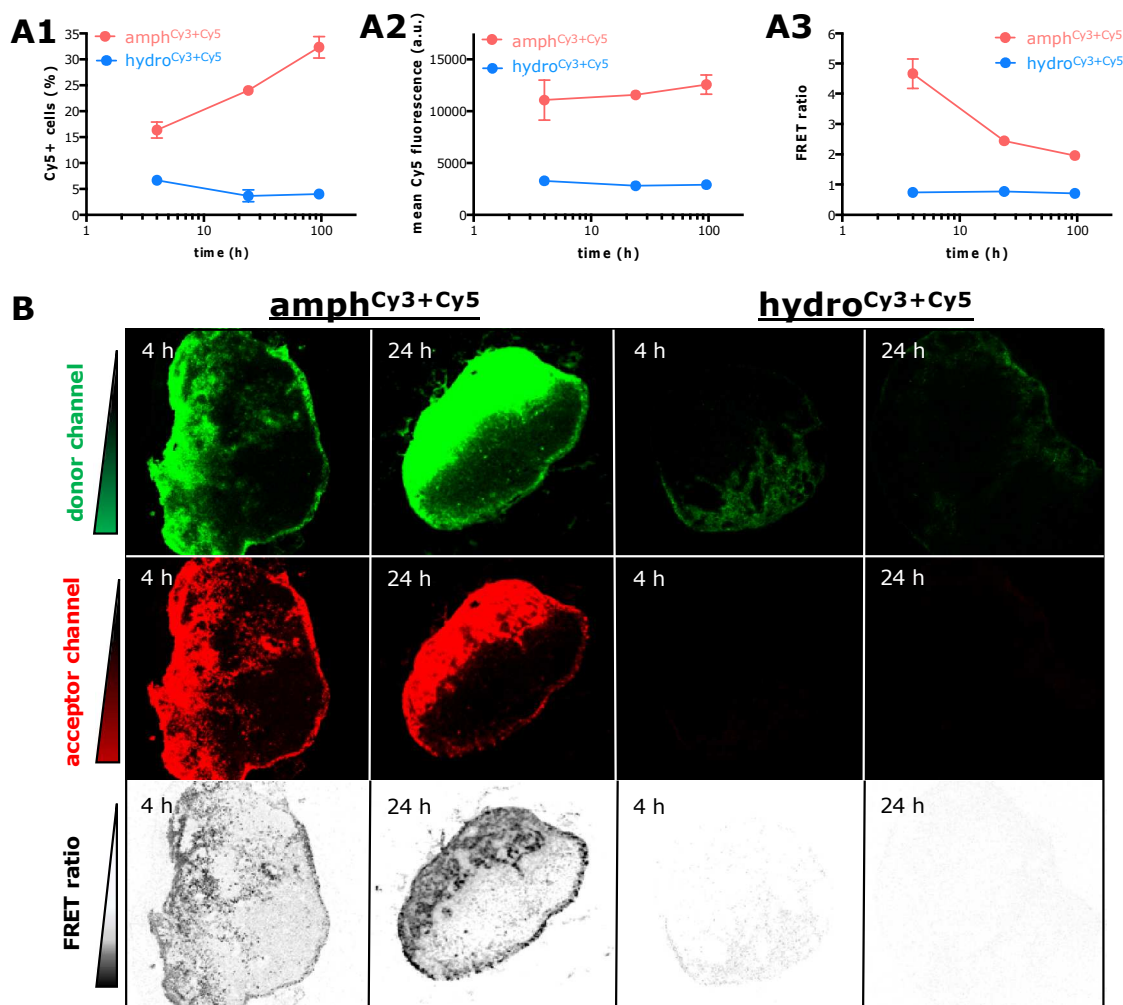


Figure 4. (A) FACS analysis of the draining popliteal lymph nodes at 4 h, 24 h and 96 h post injection. (n=3, mean + SD). (A1) percentage of Cy5-positive cells; (A2) Cy5 mean fluorescence intensity (MFI) and (A3) quantification of FRET coupling. (B) Confocal microscopy of the draining popliteal lymph nodes 4h and 24h post injection. Donor (excitation at 550 nm and detection at 575 nm), acceptor (excitation at 550 nm and detection at 670 nm) and FRET ratio (acceptor channel divided by donor channel) are shown for *amph^{Cy3+Cy5}* and *hydro^{Cy3+Cy5}*.

Next, we aimed at investigating the lymphatic transportation and immune-activation behavior of the micelles *in vivo* in mice. *Amph^{Cy3+Cy5}* and their hydrolyzed counterparts *hydro^{Cy3+Cy5}* were injected into the footpad of mice and the draining popliteal lymph nodes were dissected at 4 h, 24 h and 96 h post-injection and analyzed by confocal microscopy on histology sections and by FACS on single cell suspensions (**Figure 4**). Confocal microscopy (**Figure 4B**) revealed a dramatic difference in lymphatic transportation between *Amph^{Cy3+Cy5}* and *hydro^{Cy3+Cy5}*, showing massive translocation to the draining lymph nodes of the micelles, as early as 4 h post injection. At 4h post injection, most of the fluorescence signal was observed in the subcapsular sinus and underlying B cell follicles of the draining lymph nodes, an intranodal biodistribution generally observed for small sized particles that reach the

lymph nodes via passive transport through the afferent lymphatics.^{6,8} A similar intranodal distribution was apparent at 24 hours post injection, with an increased fluorescence intensity confirming the flow cytometry data.

Strikingly, also on tissue sections strong FRET coupling could be observed in case of *Amph^{Cy3+Cy5}* (**Figure 4B**), which gradually vanished over time and which was absent in case of *hydro^{Cy3+Cy5}*, suggesting that the block copolymer amphiphiles largely remain in micelle-assembled state during transportation from the site of injection to the lymph nodes. We hypothesize that upon arrival in lymph nodes at the subcapsular sinuses, the micelles become endocytosed by immune cells and gradually disassembly into unimers through endosomal pH induced hydrolysis of the ketal bonds that connect the benzyl moieties to the polymer backbone. Our present findings

are intriguing in view of earlier reports by the Irvine group who found that oligonucleotide-lipid amphiphiles (in particular based on dialkyl lipids conjugated to the oligonucleotide TLR9 agonist CpG) composed of a hydrophobic aliphatic tail with strong tendency to disassemble in physiological medium thereby rapidly binding to albumin (referred to as ‘albumin hitch hiking’), exhibited superior lymphatic transportation compared to more stabilized structures.²⁵ The case we present in this paper strongly differs from the Irvine structures as it comprises highly stable block copolymer micelles that remain – based on our FRET data – largely intact upon dilution and with high resilience to albumin-induced disassembly, are also great performers in terms of lymphatic transportation. Measuring binding affinity between albumin and respectively **amph** and **hydro** by bio-layer interferometry (Figure S12) revealed that **amph** had a lower affinity than **hydro** towards adsorption onto albumin-functionalized sensors. These findings further support the hypothesis that interaction with albumin is likely not the driving force for lymphatic accumulation of the amphiphilic block copolymer structures reported in this paper. Our current observations provide further insights on how to engineer synthetic macromolecular carriers to modulate the pharmacokinetic profile of biologically active molecules, in particular in the context of targeting lymphoid tissue. Of note, improved lymphatic transportation of nanoparticles over soluble hydrophilic polymers is a reported phenomenon.^{6,16}

FACS analysis provided further quantitative proof of intact micelle lymphatic transportation followed by endocytosis by immune cells and gradual intracellular micelle disassembly. Indeed, a striking difference in both the percentage of Cy5 positive cells and the mean fluorescence intensity (MFI) is observed between **amph**^{Cy3+Cy5} and **hydro**^{Cy3+Cy5} (Figure 4A), which is much higher than the observed difference in endocytosis *in vitro*. The percentage of Cy5 micelle positive lymphocytes further increases over time with the MFI values remaining constant, hence, suggesting a continuous flow of micelles from the site of injection to the lymph nodes.

To assess whether enhanced lymphatic translocation of **amph** is also translated in lymph node focused immune activation, we first assessed the spatial distribution of the

type I interferon response induced by TLR triggering of conjugated IMDQ TLR7/8 agonist. Hereto we used IFN β +/ $\Delta\beta$ -luc luciferase reporter mice,²⁶ with a reporter gene linked to the expression of the type I interferon, IFN β . IMDQ in soluble form, in **amph**^{IMDQ} and **hydro**^{IMDQ} conjugated form were injected into the footpad of mice followed by non-invasive full body luminescence imaging after 4 and 24 h. As control, non-IMDQ containing micelles, **amph**^{BZ}, were used. 4 h post-injection a strong systemic inflammatory response was observed, in response to injection of IMDQ in soluble form, which is in line with earlier reports on the fast biodistribution of small molecules TLR agonists.⁵⁻⁷ This type I IFN response remained after 24 h with strong signal resulting from major organs and the neck, with a low fraction of local activation in the draining popliteal lymph node compared to the full body luminescence (Figure 5A and Figure S17). In contrast, **amph**^{IMDQ} provoked a strong lymph node localized response. In good agreement with the microscopy and FACS data, **amph**^{IMDQ} largely outperforms **hydro**^{IMDQ} in terms of immune activation in the lymph nodes in terms of the differential luminescence intensity at the draining lymph node relative to the systemic response. Interestingly, **hydro**^{IMDQ} does not efficiently accumulate in the lymph node (*cf.* FACS and microscopy data) and mainly provokes immune activation at the site of injection, but neither provokes localized nor systemic immune activation. The question whether **hydro**^{IMDQ} itself shows a higher tendency to distribute systemically remain elusive. However, the slightly lower extent of endocytosis of **hydro** *in vitro*, might also account for its reduced activity *in vivo*.

To assess whether the IFN response results in potent activation of antigen presenting cells in the lymph nodes, mice were injected with IMDQ in soluble, **amph**^{IMDQ} and **hydro**^{IMDQ} conjugated form. Subsequently, the relative number of lymphocytes in the draining popliteal lymph node was counted as well as the extent of maturation (characterized by expression of the maturation markers CD40 and CD86) in the DC population. As shown in Figure 5B, **amph**^{IMDQ} outperforms IMDQ both as **hydro**^{IMDQ} and in soluble form. Increased influx and presence of activated DCs in the lymph nodes temporarily shuts down

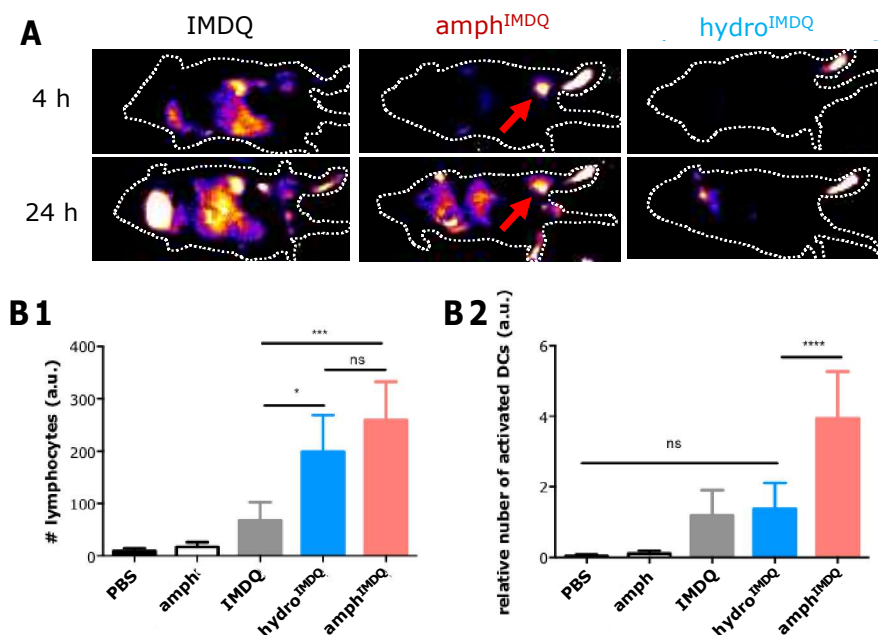


Figure 5. (A) Representative luminescence images of luciferase reporter mice ($\text{IFN}\beta^+/\Delta\beta\text{-luc}$), images taken 4h and 24 h after footpad injection of soluble IMDQ, $\text{amph}^{\text{IMDQ}}$ or $\text{hydro}^{\text{IMDQ}}$. (B) FACS analysis of the draining popliteal lymph nodes after footpad injection of the soluble IMDQ, $\text{amph}^{\text{IMDQ}}$ or $\text{hydro}^{\text{IMDQ}}$, amph^{Bz} or PBS ($n=4$, mean + SD). (B1) Analysis on total lymphocyte count and (B2) activated dendritic cells (CD11c^+ , MHCII^+ , CD40^+ , CD86^+ cells). ($n=4$, mean + SD).

lymphocyte expression from the lymph nodes to maximize chances of productive DC-T cell encounters and are likely the cause of the increased lymphocyte numbers observe in **Figure 5B1**. These findings highlight once more the tremendous potential of delivery strategies to alter the pharmacokinetic and pharmacodynamics profile of small molecule immune-modulators to shift their activity from systemic to local action.

SUMMARY AND CONCLUSIONS

In conclusion, we have presented a novel type of block copolymer amphiphiles with high stability in complex physiological media, owing to aromatic repeating units. Rapid micelle-to-unimer transition takes place in response to endosomal pH conditions, due to hydrolysis of the ketal bonds between the aromates in the side chain and the polymer backbone. In vivo, upon subcutaneous injection, we found that this type of block copolymer amphiphile translocates in intact micellar form via the interstitial flow to the draining lymph nodes, where it is internalized by immune cells. This is in stark contrast with earlier reports on lipid based amphiphiles than whose lymphatic drainage properties strongly depend on micelle disassembly and albumin binding.²⁵ Covalent conjugation of a potent small molecule TLR7/8 agonist to the hydrophobic polymer block allowed for efficient lymph mode restricted immune activation and avoids the systemic inflammatory response induced by the same TLR7/8 agonist in soluble form. The low immune-activation potential of this type of TLR7/8 agonist carrier system in unimer form is attractive in view of avoiding long term inflammatory responses, as once the amphiphilic polymer is degraded into soluble unimers their

inflammatory activity is reduced and the soluble nature of the polymer should favor renal secretion and hence avoid accumulation in the body. Our findings provide novel insights with regard to macromolecular and supramolecular design of biomaterials for immune-engineering.

ASSOCIATED CONTENT

Supporting Information. Experimental details and additional data. This material is available free of charge via the Internet at <http://pubs.acs.org>.

AUTHOR INFORMATION

Corresponding Author

* br.degeest@ugent.be

Present Addresses

†Max Planck Institute for Polymer Research, Mainz, Germany

Author Contributions

The manuscript was written through contributions of all authors. / All authors have given approval to the final version of the manuscript.

ACKNOWLEDGMENT

BGDG acknowledges the FWO Flanders, Ghent University (BOF-GOA) and Kom op Tegen Kanker for funding.

REFERENCES

- Palucka, K.; Banchereau, J. Cancer Immunotherapy via Dendritic Cells. *Nat. Rev. Cancer* **2012**, *12* (4), 265–277.
- Hubbell, J. a; Thomas, S. N.; Swartz, M. a. Materials Engineering for Immunomodulation. *Nature* **2009**, *462* (7272), 449–460.

- (3) Iwasaki, A.; Medzhitov, R. Control of Adaptive Immunity by the Innate Immune System. *Nat. Immunol.* **2015**, *16* (4), 343–353.
- (4) Mancini, R. J.; Stutts, L.; Ryu, K. A.; Tom, J. K.; Esser-Kahn, A. P. Directing the Immune System with Chemical Compounds. *ACS Chem. Biol.* **2014**, *9* (5), 1075–1085.
- (5) Nuhn, L.; Vanparijs, N.; De Beuckelaer, A.; Lybaert, L.; Verstraete, G.; Deswarte, K.; Lienenklaus, S.; Shukla, N. M.; Salyer, A. C. D.; Lambrecht, B. N.; Grooten, J.; David, S. A.; De Koker, S.; De Geest, B. G. PH-Degradable Imidazoquinoline-Ligated Nanogels for Lymph Node-Focused Immune Activation. *Proc. Natl. Acad. Sci.* **2016**, *113* (29), 8098–8103.
- (6) Lynn, G. M.; Laga, R.; Darrah, P. A.; Ishizuka, A. S.; Balaci, A. J.; Dulcey, A. E.; Pechar, M.; Pola, R.; Gerner, M. Y.; Yamamoto, A.; Buechler, C. R.; Quinn, K. M.; Smelkinson, M. G.; Vanek, O.; Cawood, R.; Hills, T.; Vasalatiy, O.; Kastenmüller, K.; Francica, J. R.; Stutts, L.; Tom, J. K.; Ryu, K. A.; Esser-Kahn, A. P.; Etrych, T.; Fisher, K. D.; Seymour, L. W.; Seder, R. A. In Vivo Characterization of the Physicochemical Properties of Polymer-Linked TLR Agonists That Enhance Vaccine Immunogenicity. *Nat. Biotechnol.* **2015**, *33* (11), 1201–1210.
- (7) Ignacio, B. J.; Albin, T. J.; Esser-Kahn, A. P.; Verdoes, M. Toll-like Receptor Agonist Conjugation: A Chemical Perspective. *Bioconjug. Chem.* **2018**, *29* (3), 587–603.
- (8) Moon, J. J.; Suh, H.; Bershteyn, A.; Stephan, M. T.; Liu, H.; Huang, B.; Sohail, M.; Luo, S.; Ho Um, S.; Khant, H.; Goodwin, J. T.; Ramos, J.; Chiu, W.; Irvine, D. J. Interbilayer-Crosslinked Multilamellar Vesicles as Synthetic Vaccines for Potent Humoral and Cellular Immune Responses. *Nat. Mater.* **2011**, *10* (3), 243–251.
- (9) Reddy, S. T.; Van Der Vlies, A. J.; Simeoni, E.; Angeli, V.; Randolph, G. J.; O’Neil, C. P.; Lee, L. K.; Swartz, M. A.; Hubbell, J. A. Exploiting Lymphatic Transport and Complement Activation in Nanoparticle Vaccines. *Nat. Biotechnol.* **2007**, *25* (10), 1159–1164.
- (10) Yoo, E.; Salyer, A. C. D.; Brush, M. J. H.; Li, Y.; Trautman, K. L.; Shukla, N. M.; De Beuckelaer, A.; Lienenklaus, S.; Deswarte, K.; Lambrecht, B. N.; De Geest, B. G.; David, S. A. Hyaluronic Acid Conjugates of TLR7/8 Agonists for Targeted Delivery to Secondary Lymphoid Tissue. *Bioconjug. Chem.* **2018**, *29* (8), 2741–2754.
- (11) Vanparijs, N.; Nuhn, L.; De Geest, B. G. Transiently Thermoresponsive Polymers and Their Applications in Biomedicine. *Chem. Soc. Rev.* **2017**, *46* (4), 1193–1239.
- (12) Binauld, S.; Stenzel, M. H. Acid-Degradable Polymers for Drug Delivery: A Decade of Innovation. *Chem. Commun.* **2013**, *49* (21), 2082.
- (13) Liu, B.; Thayumanavan, S. Substituent Effects on the PH Sensitivity of Acetals and Ketals and Their Correlation with Encapsulation Stability in Polymeric Nanogels. *J. Am. Chem. Soc.* **2017**, *139* (6), 2306–2317.
- (14) Stuart, M. a C.; Huck, W. T. S.; Genzer, J.; Müller, M.; Ober, C.; Stamm, M.; Sukhorukov, G. B.; Szleifer, I.; Tsukruk, V. V.; Urban, M.; Winnik, F.; Zauscher, S.; Luzinov, I.; Minko, S. Emerging Applications of Stimuli-Responsive Polymer Materials. *Nat. Mater.* **2010**, *9* (2), 101–113.
- (15) Nuhn, L.; Van Herck, S.; Best, A.; Deswarte, K.; Kokkinopoulou, M.; Lieberwirth, I.; Koynov, K.; Lambrecht, B. N.; De Geest, B. G. FRET Monitoring of Intracellular Ketal Hydrolysis in Synthetic Nanoparticles. *Angew. Chemie Int. Ed.* **2018**, *57* (33), 10760–10764.
- (16) Nuhn, L.; Van Hoecke, L.; Deswarte, K.; Schepens, B.; Li, Y.; Lambrecht, B. N.; De Koker, S.; David, S. A.; Saelens, X.; De Geest, B. G. Potent Anti-Viral Vaccine Adjuvant Based on PH-Degradable Nanogels with Covalently Linked Small Molecule Imidazoquinoline TLR7/8 Agonist. *Biomaterials* **2018**, *178*, 643–651.
- (17) Bachmann, M. F.; Jennings, G. T. Vaccine Delivery: A Matter of Size, Geometry, Kinetics and Molecular Patterns. *Nat. Rev. Immunol.* **2010**, *10* (11), 787–796.
- (18) Shi, Y.; van der Meel, R.; Theek, B.; Oude Blenke, E.; Pieters, E. H. E.; Fens, M. H. A. M.; Ehling, J.; Schiffelers, R. M.; Storm, G.; van Nostrum, C. F.; Lammers, T.; Hennink, W. E. Complete Regression of Xenograft Tumors upon Targeted Delivery of Paclitaxel via Π - Π Stacking Stabilized Polymeric Micelles. *ACS Nano* **2015**, *9* (4), 3740–3752.
- (19) Kierstead, P. H.; Okochi, H.; Venditto, V. J.; Chuong, T. C.; Kivimae, S.; Fréchet, J. M. J.; Szoka, F. C. The Effect of Polymer Backbone Chemistry on the Induction of the Accelerated Blood Clearance in Polymer Modified Liposomes. *J. Control. Release* **2015**, *213*, 1–9.
- (20) Roy, R.; Hohng, S.; Ha, T. A Practical Guide to Single-Molecule FRET. *Nat. Methods* **2008**, *5* (6), 507–516.
- (21) Lu, J.; Owen, S. C.; Shoichet, M. S. Stability of Self-Assembled Polymeric Micelles in Serum. *Macromolecules* **2011**, *44* (15), 6002–6008.
- (22) Sun, X.; Wang, G.; Zhang, H.; Hu, S.; Liu, X.; Tang, J.; Shen, Y. The Blood Clearance Kinetics and Pathway of Polymeric Micelles in Cancer Drug Delivery. *ACS Nano* **2018**, *12* (6), 6179–6192.
- (23) Talelli, M.; Barz, M.; Rijcken, C. J. F.; Kiessling, F.; Hennink, W. E.; Lammers, T. Core-Crosslinked Polymeric Micelles: Principles, Preparation, Biomedical Applications and Clinical Translation. *Nano Today* **2015**, *10* (1), 93–117.
- (24) Canton, I.; Battaglia, G. Endocytosis at the Nanoscale. *Chem. Soc. Rev.* **2012**, *41* (7), 2718.
- (25) Liu, H.; Moynihan, K. D.; Zheng, Y.; Szeto, G. L.; Li, A. V.; Huang, B.; Van Egeren, D. S.; Park, C.; Irvine, D. J. Structure-Based Programming of Lymph-Node Targeting in Molecular Vaccines. *Nature* **2014**, *507* (7493), 519–522.
- (26) Lambrecht, L.; Vanvarenberg, K.; De Beuckelaer, A.; Van Hoecke, L.; Grooten, J.; Ucakar, B.; Lipnik, P.; Sanders, N. N.; Lienenklaus, S.; Pr at, V.; Vandermeulen, G. Coadministration of a Plasmid Encoding HIV-1 Gag Enhances the Efficacy of Cancer DNA Vaccines. *Mol. Ther.* **2016**, *24* (9), 1686–1696.

Graphic entry for the Table of Contents (TOC)

